

‘Melt welt’ mechanism of extreme weakening of gabbro at seismic slip rates

Kevin M. Brown¹ & Yuri Fialko¹

Laboratory studies of frictional properties of rocks at slip velocities approaching the seismic range (~ 0.1 – 1 m s^{-1}), and at moderate normal stresses (1–10 MPa), have revealed a complex evolution of the dynamic shear strength, with at least two phases of weakening separated by strengthening at the onset of wholesale melting^{1–4}. The second post-melting weakening phase is governed by viscous properties of the melt layer and is reasonably well understood^{5,6}. The initial phase of extreme weakening, however, remains a subject of much debate. Here we show that the initial weakening of gabbro is associated with the formation of hotspots and macroscopic streaks of melt (‘melt welts’), which partially unload the rest of the slip interface. Melt welts begin to form when the average rate of frictional heating exceeds 0.1 – 0.4 MW m^{-2} , while the average temperature of the shear zone is well below the solidus (250–450 °C). Similar heterogeneities in stress and temperature are likely to occur on natural fault surfaces during rapid slip, and to be important for earthquake rupture dynamics.

Several mechanisms have been proposed to explain the pre-melting weakening, including flash melting^{7,8}, lubrication by hydrous films coating the gouge particles^{9,10}, silica gel formation², nano-powder lubrication, thermal decomposition and degassing¹¹. Of the proposed mechanisms, only the first two could potentially explain extreme weakening in crystalline mafic rocks^{1,4}. To investigate the nature of extreme dynamic weakening before the onset of wholesale melting, we performed a series of medium- to high-speed friction experiments on diabase (fine-grained gabbro). The tests were conducted using a rotary shear apparatus (see Methods for details of the experimental setup). Figure 1 shows a typical experimental record. At velocities well below the critical value (defined below) of $\sim 0.1 \text{ m s}^{-1}$, the coefficient of friction drops by 10–20% from a peak static value to a nearly constant kinetic value of ~ 0.6 – 0.8 —consistent with Byerlee’s law¹²—within a few tens of seconds, or a slip distance of several metres. Our focus in this study, however, is a subsequent dramatic weakening that reduces the effective coefficient of friction by a factor of 2 or more (Fig. 1 and Supplementary Fig. 2). This extreme weakening is observed above a critical velocity V_c of ~ 0.06 – 0.2 m s^{-1} , in agreement with previously reported high-speed friction data^{1–4}. Most of our tests were conducted near the critical velocity V_c to explore relationships between V_c , the normal stress, the slip distance, and the average temperature of the shear zone. The tests revealed a systematic decrease in V_c with increasing normal stress (Supplementary Fig. 3). The boundary between weakened and unweakened regimes is fairly sharp; near this boundary, a velocity increment of as little as 10^{-2} m s^{-1} is often sufficient to trigger weakening, and the critical increment appears to decrease at higher normal stress (Supplementary Fig. 3). The observed dependence of the onset of weakening on normal stress (Supplementary Fig. 3) and slip distance (Fig. 1 and Supplementary Fig. 2) is suggestive of a thermally activated mechanism. Figure 2 shows the dissipative power density (work done against friction per unit slip area per unit time, τV , where τ is the average shear stress, and V is the slip velocity) plotted against the time to the onset of weakening, t_c . The data reveal a critical power density, demarcating the boundary between the weakened and

unweakened states, of ~ 0.1 – 0.4 MW m^{-2} , in agreement with previous estimates¹³. The power density associated with seismic ruptures, $\tau V \approx (10^1$ – $10^2) \text{ MW m}^{-2}$, greatly exceeds the critical power density inferred from laboratory data (Fig. 2), so the experimentally deduced conditions for the onset of weakening are certainly met during natural earthquakes, provided that seismic slip is sufficiently localized^{14,15}. The time until the onset of weakening, t_c , is greatly reduced if frictional losses τV exceed the critical power density τV_c .

To investigate the nature of the weakening mechanism, we evaluated temperature on the slip interface using a combination of direct temperature measurements inside the sample and numerical modelling (see Methods). Figure 3 shows the observed critical velocity, V_c , as a function of the background temperature of the shear zone, T_b , at the onset of weakening. As can be seen in Fig. 3, weakening occurs when the average temperature of the shear zone varies from ~ 270 – 350 °C (at normal stress of ~ 1 MPa and slip rate greater than 0.1 m s^{-1}) to ~ 450 – 550 °C (at normal stress of ~ 4 – 5 MPa and slip rate less than 0.1 m s^{-1}). These average temperatures are well above the boiling point of aqueous fluids, thus ruling out processes associated with nano-layers of absorbed water on fine gouge particles^{9,10}. The data shown in Fig. 3 can be also used to test the flash melting hypothesis^{7,8}. Flash melting is believed to occur when the heat generated from rubbing of microscopic, highly stressed asperities is sufficient to thermally weaken the asperities on a timescale of a transient contact. The critical weakening velocity V_c at the onset of flash melting is given by⁷

$$V_c = \frac{\pi \kappa}{a} \left(\frac{\rho c (T_w - T_b)}{\tau_c} \right)^2 \quad (1)$$

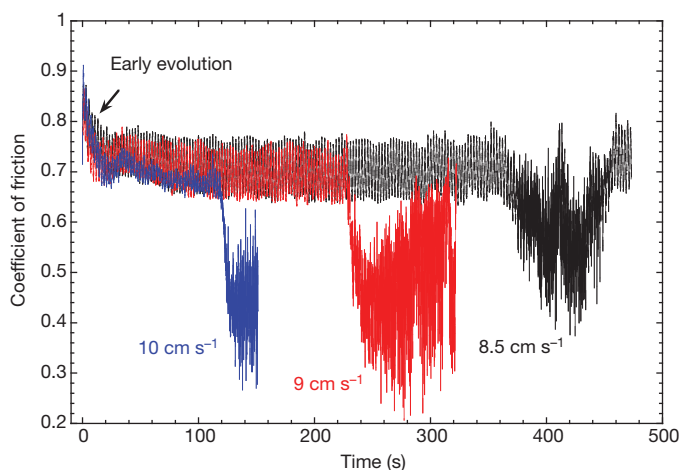


Figure 1 | Experimentally measured evolution of the coefficient of friction at three different ‘near-critical’ velocities. Blue, red and black lines show data from tests 90.31, 90.32 and 90.33, respectively (see Supplementary Table 1), with velocities as labelled. Normal stress equals 3 MPa. Note the onset of strong dynamic weakening at ~ 120 , 230 and 360 s, respectively.

¹Institute of Geophysics and Planetary Physics, Scripps Institution of Oceanography, University of California, San Diego, La Jolla, California 92093, USA.

where a is the characteristic size of contacts, κ is thermal diffusivity, c is specific heat, ρ is density, τ_c is the characteristic strength of contacts, and T_w is the weakening temperature, at which contacts lose strength. The flash melting hypothesis predicts that the critical weakening velocity should be independent of normal stress, in apparent contradiction with observations shown in Supplementary Fig. 3. Note, however, that higher normal stress can affect the onset of weakening indirectly, through increases in ambient temperature T_b . We used equation (1) to calculate the critical weakening velocity predicted by the flash melting model, assuming that the background temperature equals the estimated temperature of the shear zone at the onset of weakening. The respective model predictions are shown in Fig. 3. The best-fitting values of the asperity size a (2–5 μm) are within the observed range of gouge particle sizes in our scanning electron microscope (SEM) images (1–10 μm ; see Fig. 4b—note that there is a poorly resolved nanoscale component in the wear products), so the flash melting hypothesis can in principle explain the inverse scaling of weakening velocity with normal stress (Supplementary Fig. 3). However, additional observations suggest that a different physical mechanism may be responsible for the strong dynamic weakening in our experiments. Stopping slip just after the onset of weakening revealed dark glassy streaks of sub-millimetre width (hereafter referred to as ‘melt welts’; Fig. 4a and Supplementary Fig. 7a), indicating the onset of macroscopic melting. Further increases in velocity, normal stress or slip duration resulted in coalescence and expansion of melt streaks into broader rings (Supplementary Figs 7b,c). We propose that the observed melt welts (Fig. 4, Supplementary Fig. 7) result from stress heterogeneities that spontaneously develop and grow on the slip interface, possibly owing to a feedback between local temperature increases and thermal expansion. We verified this hypothesis by placing temperature sensors 2 mm away from the shear zone, spanning the ring-shaped sample both across and along the slip direction (Fig. 5). These measurements showed that below the critical velocity, or before weakening, the temperature of the slip interface increases relatively uniformly. A sharp transition to a highly heterogeneous temperature distribution then occurs at time t_c , corresponding to the onset of weakening (Fig. 5). This behaviour may be similar to ‘hotspotting’ in brakes and clutches, well known in engineering tribology^{16–18}. If so, this mechanism is different from flash melting^{7,19,20} in that regions of high temperature do not need to be microscopic, highly transient and

uniformly distributed on the slip interface. By comparing temperature records from thermocouples to the location of glassy streaks in experiments stopped shortly after the onset of weakening, we confirmed that, on weakening, elevated temperatures were localized near melt welts, while the surrounding areas of the slip interface cooled. Anti-correlated variations in temperature across the ring sample in the post-weakening regime over a period of several seconds (Fig. 5) indicate that hotspots can migrate across the slip interface, presumably marking the birth and destruction of incipient melt welts.

Melt welts initially occupy a small fraction of the total contact area (Fig. 4), and cannot appreciably reduce the effective coefficient of friction (Fig. 1) if shear stress on the rest of the contact area remains high. We therefore suggest that the observed dynamic weakening results primarily from volumetric expansion in melt welts, which reduces the effective normal stress on the rest of the slip interface. Unloading of the slip interface adjacent to melt welts is evident from dramatically reduced rates of frictional heating and reversals in temperature trends (Fig. 5). Furthermore, inspection of normal stress at the onset of weakening revealed small increases in compression (Supplementary Fig. 8), consistent with net dilation in the shear zone. We confirmed a concomitant dilation of several micrometres by precise measurements of the rate of shortening across the sample (Supplementary Fig. 9).

We speculate that hotspots may initially develop as a result of a positive feedback between heating and dilatancy (for example, thermoelastic instability^{17,18}) or at the site of local stress concentrators such as ploughing gouge particles (much like galling in metals²¹; see Fig. 4) that are sufficiently long-lived to raise local temperature by several hundred degrees and initiate melting. Thus, the onset of weakening is controlled by both the average temperature of the slip zone (which increases during slip) and the transient heating of hotspots. The resulting melt welts may undergo further dilation owing to a volume increase associated with the phase change. A net reduction in the effective coefficient of friction may occur if normal stress on the unmelted part of the slip interface decreases while shear stress within melt welts does not increase in proportion to the locally increased normal stress. An important question is whether melt welts can maintain excess pressure over time. In the case of shear between two rigid surfaces, pressurized patches of melt should eventually be smeared across the slip interface. However, in the presence of gouge, lateral

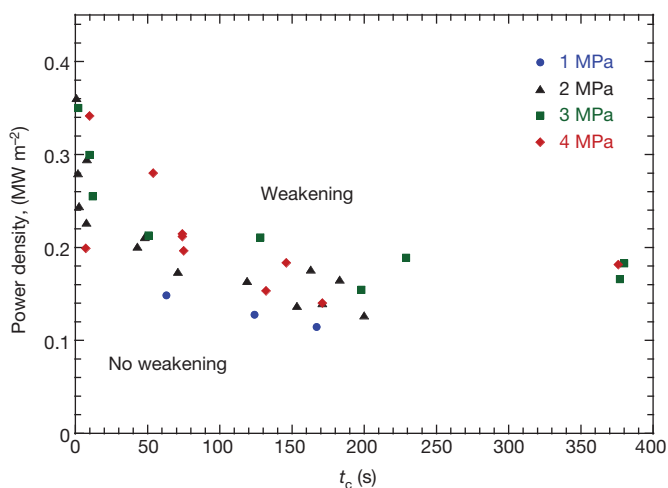


Figure 2 | Power density versus time until the onset of weakening, for experiments at four different values of normal stress. The normal stress (coloured symbols) is held constant during each experiment. Delayed weakening (larger t_c) is associated with lower power density, possibly owing to elevated temperature of the slip interface and interplay between rate- and temperature-dependent weakening mechanisms. Rapid weakening occurs when power density exceeds the threshold value denoted by coloured symbols, whereas no weakening is expected at lower values of power density.

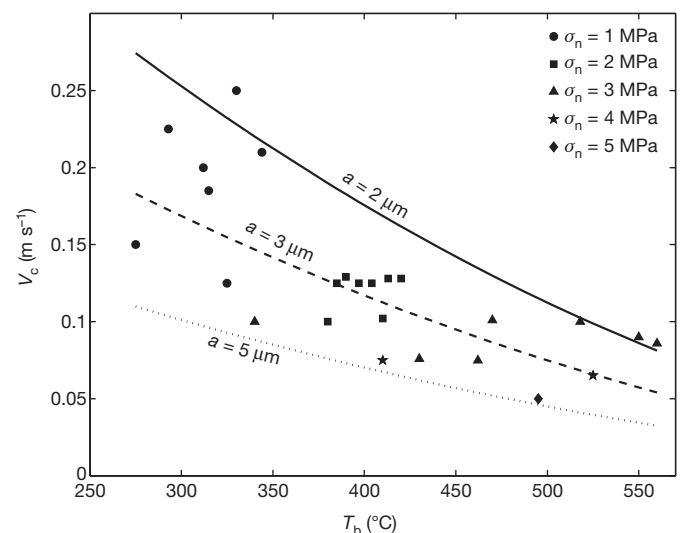


Figure 3 | Observed critical slip velocity as a function of the estimated average temperature of the slip interface at the time of weakening. Symbols denote normal stress; lines show predictions of the flash melting model (equation (1)) for different assumed values of the asperity size a . Other parameters used in the calculations include: $\tau_c = 3 \text{ GPa}$, $T_w = 900 \text{ }^\circ\text{C}$ (ref. 7), and a thermal diffusivity of $5.5 \times 10^{-7} \text{ m}^2 \text{ s}^{-2}$ (see Supplementary Table 2).

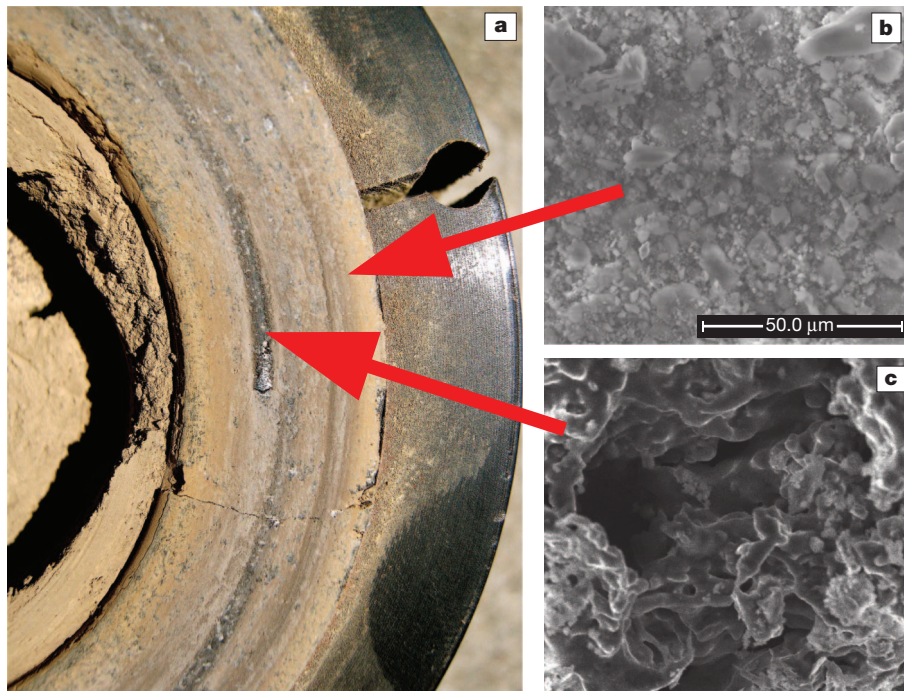


Figure 4 | Initiation of melt wets at the slip interface during the onset of dynamic weakening. Data from test 97.4. **a**, Photograph of the slip interface. **b**, **c**, SEM images of the areas shown by red arrows in **a**. **b**, Regular, unmolten

surface. Note gouge particles. **c**, Glassy streak area. Dark, smooth surfaces, a scarcity of clasts, and 'ropy' flow structures are indicators of local melting. Scale bar, 50 μm ; same scale applies to panel **c**.

propagation of melt blobs may be limited by the strength of the gouge layer. The melt extrusion would require displacement (or absorption) of the gouge particles ahead of the advancing melt front, thus allowing melt wets to maintain excess pressure and push the shear zone apart. Increases in slip velocity, normal stress or total slip distance lead to widening and coalescence of melt wets (Supplementary Fig. 7), and ultimately to wholesale melting. As growing melt wets occupy a progressively larger fraction of the slip interface, thereby increasing

the true contact area and reducing the contribution of unmelted (low-normal-stress) contact, the average shear stress may increase. The onset of strengthening in our experiments is manifested by visible flashes at the edges of the slip zone, and the peak strength is associated with formation of a continuous, through-going layer of melt that covers the entire contact, in agreement with previously published results^{1,3,4}. Note that transient strengthening before wholesale melting observed in high-speed, low-normal-stress friction experiments cannot be readily explained by the flash melting model. We also point out that the melt-welt mechanism does not require an extreme strain localization in the gouge layer, nor special assumptions about the size and strength of gouge particles.

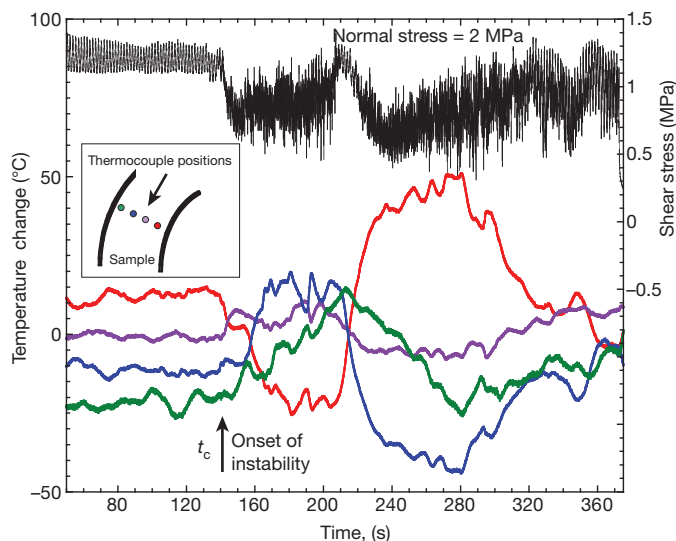


Figure 5 | Evolution of shear stress and temperature through the onset of weakening. Black line, right axis: measured shear stress. Coloured lines, left axis: temperature deviations recorded by individual thermocouples with respect to the mean value for the four thermocouples ($\sim 280^\circ\text{C}$), at 2 mm distance from the slip interface. Thermocouple positions are shown in the inset. Note anticorrelated variations in temperature (for example, blue and red lines), probably indicating initiation and termination of melt wets at different locations on the interface. Data from test 98.20; slip velocity $V = 0.125 \text{ m s}^{-1}$.

It is reasonable to assume that if extreme stress and temperature heterogeneities are developing and growing spontaneously on a nominally flat frictional interface in carefully controlled laboratory experiments, they are also present on rough fault surfaces during seismic slip. Extrapolation of critical velocities measured in our experiments to conditions at the base of the brittle layer, where most large earthquakes nucleate, implies that strong dynamic weakening may occur at much earlier stages of seismic rupture than commonly believed. Assuming that the slip instability is highly localized and that the scalings inferred from low-normal-stress data (Fig. 2, Supplementary Fig. 3) hold, strong dynamic weakening at seismogenic depths may initiate at slip velocities as small as several millimetres per second. At low normal stress, the melt-welt mechanism may induce strong dynamic weakening on shallow parts of seismogenic faults that are nominally velocity-strengthening and prone to creep in the interseismic period. The onset of melt-welt weakening requires the rate of energy dissipation on a slip interface to be greater than $\sim 0.1\text{--}0.35 \text{ MW m}^{-2}$ (Fig. 2). These values are similar to the critical power density reported in a recent compilation of high-speed laboratory measurements of rock friction¹³. Further experimental studies (in particular, at higher normal stress) are required to verify if the data shown in Fig. 2 and Supplementary Fig. 3 can indeed be extrapolated. The proposed mechanism does not preclude the occurrence of other potential mechanisms of strong dynamic weakening (for example, aquathermal pressurization). In fact, such additional mechanisms may be required

to reconcile the inferred low dynamic strength of earthquake ruptures with the scarcity of pseudotachylites on exhumed natural faults^{5,7,22,23}.

METHODS SUMMARY

Our high-speed friction experiments were conducted on a modified industrial lathe (Supplementary Fig. 1) at normal stresses between 0.5 and 5 MPa and slip velocities of 10^{-2} to 0.5 m s^{-1} . The rock samples consisted of a ring with internal diameter $D_1 = 54 \text{ mm}$ and external diameter $D_2 = 80 \text{ mm}$ on the rotating side of the apparatus, and a square plate on the stationary side embedded within the non-rotating flywheel (Supplementary Fig. 1). Both the ring and the plate are 12 mm thick. The ring geometry was chosen to minimize variations in slip rate and temperature across the slip interface. To monitor frictional heating and temperature variations inside the sample, we placed thermocouples in small holes drilled laterally into the side of the non-rotating plate at three different distances from the slip interface, as well as at four positions equally spaced across the sample in the radial direction at 2 mm distance from the slip interface (Fig. 5 inset). Numerical simulations were performed using the finite-element program Abaqus/Simulia²⁴.

Full Methods and any associated references are available in the online version of the paper.

Received 14 December 2011; accepted 29 June 2012.

1. Tsutsumi, A. & Shimamoto, T. High-velocity frictional properties of gabbro. *Geophys. Res. Lett.* **24**, 699–702 (1997).
2. Goldsby, D. & Tullis, T. Low frictional strength of quartz rocks at subseismic slip rates. *Geophys. Res. Lett.* **29** (2002).
3. Di Toro, G., Goldsby, D. L. & Tullis, T. E. Friction falls towards zero in quartz rock as slip velocity approaches seismic rates. *Nature* **427**, 436–439 (2004).
4. Hirose, T. & Shimamoto, T. Fractal dimension of molten surfaces as a possible parameter to infer the slip-weakening distance of faults from natural pseudotachylites. *J. Struct. Geol.* **25**, 1569–1574 (2003).
5. Fialko, Y. & Khazan, Y. Fusion by earthquake fault friction: Stick or slip? *J. Geophys. Res.* **110**, B12407 (2005).
6. Nielsen, S., Di Toro, G., Hirose, T. & Shimamoto, T. Frictional melt and seismic slip. *J. Geophys. Res.* **113**, B01308 (2008).
7. Rice, J. R. Heating and weakening of faults during earthquake slip. *J. Geophys. Res.* **111**, B05311 (2006).
8. Goldsby, D. & Tullis, T. Flash heating leads to low frictional strength of crustal rocks at earthquake slip rates. *Science* **334**, 216–218 (2011).
9. Reches, Z. & Lockner, D. A. Fault weakening and earthquake instability by powder lubrication. *Nature* **467**, 452–455 (2010).
10. Sammis, C., Lockner, D. & Reches, Z. The role of adsorbed water on the friction of a layer of submicron particles. *Pure Appl. Geophys.* **168**, 2325–2334 (2011).
11. Han, R., Shimamoto, T., Hirose, T., Ree, J.-H. & Ando, J. Ultralow friction of carbonate faults caused by thermal decomposition. *Science* **316**, 878–881 (2007).
12. Byerlee, J. Friction of rock. *Pure Appl. Geophys.* **116**, 615–626 (1978).
13. Di Toro, G. *et al.* Fault lubrication during earthquakes. *Nature* **471**, 494–498 (2011).
14. Chester, F. M. & Chester, J. S. Ultracataclastic structure and friction processes of the Punchbowl fault, San Andreas system, California. *Tectonophysics* **295**, 199–221 (1998).
15. Fialko, Y. Temperature fields generated by the elastodynamic propagation of shear cracks in the Earth. *J. Geophys. Res.* **109**, B01303 (2004).
16. Dow, T. Thermoelastic effects in a thin sliding seal — a review. *Wear* **59**, 31–52 (1980).
17. Anderson, A. & Knapp, R. Hot spotting in automotive friction systems. *Wear* **135**, 319–337 (1990).
18. Lee, K. & Barber, J. Frictionally excited thermoelastic instability in automotive disk brakes. *J. Tribol.* **115**, 607–614 (1993).
19. Bowden, F. B. & Persson, P. A. Deformation heating and melting of solids in high speed friction. *Proc. R. Soc. Lond. A* **260**, 433–458 (1960).
20. Molinari, A., Estrin, Y. & Mercier, S. Dependence of the coefficient of friction on the sliding conditions in the high velocity range. *J. Tribol.* **121**, 35–41 (1999).
21. Schedin, E. & Lehtinen, B. Galling mechanisms in lubricated systems: a study of sheet metal forming. *Wear* **170**, 119–130 (1993).
22. Brune, J. N., Henyey, T. & Roy, R. Heat flow, stress, and rate of slip along San Andreas fault, California. *J. Geophys. Res.* **74**, 3821–3827 (1969).
23. Lapusta, N., Rice, J. R., Ben-Zion, Y. & Zheng, G. Elastodynamic analysis for slow tectonic loading with spontaneous rupture episodes on faults with rate- and state-dependent friction. *J. Geophys. Res.* **105**, 23765–23789 (2000).
24. Abaqus/Simulia v.6.11; available at <http://www.3ds.com/products/simulia/overview/> (Dassault Systèmes, 2012).

Supplementary Information is linked to the online version of the paper at www.nature.com/nature.

Acknowledgements We thank D. Lockner for comments that improved this manuscript. The SIO Marine Science Development Center provided the lathe used in our experiments. This work was supported by NSF (grant EAR-0838255).

Author Contributions K.M.B. built the apparatus, K.M.B. and Y.F. designed and conducted experiments, Y.F. performed numerical modelling.

Author Information Reprints and permissions information is available at www.nature.com/reprints. The authors declare no competing financial interests. Readers are welcome to comment on the online version of this article at www.nature.com/nature. Correspondence and requests for materials should be addressed to K.M.B. (kmbrown@ucsd.edu) or Y.F. (yfialko@ucsd.edu).

METHODS

Our high-speed rotary friction apparatus was developed on a modified industrial lathe chassis (Supplementary Fig. 1). The apparatus allows measurements of friction at slip velocities between 0.003 and 2 m s^{-1} , normal stress up to 5 MPa, and unlimited total displacement. Modifications to the lathe chassis included removing excess components, tightening the clutch and attaching a stronger, digitally controlled drive motor. The rock samples consisted of a ring with internal diameter $D_1 = 54 \text{ mm}$ and external diameter $D_2 = 80 \text{ mm}$ on the rotating side of the apparatus, and a square plate on the stationary side embedded within the non-rotating flywheel (Supplementary Fig. 1). Both the ring and the plate are 12 mm thick. The ring geometry was chosen to minimize variations in slip rate and temperature across the slip interface.

The samples were ground to an initial surface roughness of 60–80 grit and had an initial parallelism of the mating surfaces of the order of micrometres over tens of centimetres. Before each experiment, we ran the samples in for several tens of metres to develop a gouge layer (typically having thickness of a fraction of a millimetre throughout the experiment). In each experiment, the sample was first put under normal load, and then accelerated to the target speed. The reported slip velocity corresponds to that in the middle of the ring sample, $V = \pi(D_1 + D_2)\omega/2$, where ω is the revolution speed of the sample holder, in revolutions per second. Shear and normal stress were calculated by dividing the tangential and axial forces acting on a sample by the nominal contact area, $\pi(D_2^2 - D_1^2)/4$.

Considerable efforts were made to increase the stiffness and inertial dampening of the machine, to prevent chatter and high-frequency vibrations during the tests. A significant chatter was observed in the initial low-stiffness configuration of the apparatus. Sampling at high frequency ($>5,000 \text{ Hz}$) showed that the chatter in fact resulted from stick–slip behaviour, even at nominal slip rates in excess of 1 m s^{-1} . Chatter resulted in instantaneous peak slip rates an order of magnitude higher than the nominal slip speeds. After modification of the apparatus, involving stiffening of the loading shaft and adding a massive fly-wheel, most of the high-frequency chatter was suppressed. Still remaining are periodic oscillations in torque and normal stress, most likely owing to imperfectly parallel contacts (see, for example, Fig. 1 and Supplementary Fig. 2). The magnitude of the oscillations typically changes with time, increasing and decreasing as wear modifies the geometry of the slip interface. The onset of weakening in our experiments is manifested in a transition to irregular, high-frequency oscillations (Supplementary Fig. 4), and sometimes a barely audible rumble.

Because temperature on the slip interface could not be measured directly, we evaluated the average surface temperature using a numerical model constrained by temperature measurements inside the sample. Thermocouples were placed in small holes drilled laterally into the side of the non-rotating plate at three different distances from the slip interface, equally spaced along the contact with the ring

sample, as well as at four positions equally spaced across the sample in the radial direction at 2 mm distance from the slip interface (Fig. 5 inset).

Our model explicitly accounted for frictional heating on the slip interface, unsteady heat transfer inside the apparatus, and convective cooling on the external surfaces. We assumed axial symmetry and built a finite-element mesh of the rock sample, sample holder and adjacent parts of the apparatus (Supplementary Fig. 5). The model used experimentally measured time-dependent shear stress τ and slip velocity V as input to calculate the rate of mechanical energy done against friction (τV). The latter was applied as a heat-flux boundary condition on the slip interface, assuming that all mechanical energy is ultimately transferred into heat. A good agreement between the modelled and observed temperatures inside the sample (Supplementary Fig. 6) confirmed that frictional losses are converted primarily to thermal energy, and that surface energy associated with production of gouge particles is negligible. Convective cooling at the contacts with air was taken into account using the Robin boundary condition, $q = h(T - T_a)$, where q is the heat flux across the surface, $h = 30 \text{ W m}^{-2} \text{ }^\circ\text{C}^{-1}$ is the heat transfer coefficient, and $T_a = 22 \text{ }^\circ\text{C}$ is the ambient air temperature. We used the ‘gap conductance’ boundary condition at the contacts between the sample and sample holder, with the heat transfer coefficient proportional to the applied normal stress. Supplementary Table 2 summarizes the thermophysical properties of gabbro and steel used in our simulations. The model parameters were calibrated using data from low-speed experiments, in which no strong weakening occurred. Supplementary Fig. 6 shows a validation example in which temperatures observed in one of the experimental runs (not used to calibrate the model parameters) are compared to model predictions at the respective positions of temperature sensors inside the sample. A good agreement between the observed and calculated temperatures implies that inferences of average temperature on the shear interface are robust.

To measure the rate of wear and to verify the inferred dilatancy of the shear zone at the onset of weakening, we attached three linear variable differential transformers (LVDTs), two equidistant on either side of the sample (see Supplementary Fig. 1), and the third, with somewhat lower resolution, at a right angle to the first two, so that we could average the result to get the net axial displacement. The precision LVDTs have a maximum resolution of 0.5–1 μm , depending on integration time (typically 0.0167 Hz), and on the full voltage range setting chosen. LVDT measurements indicated that the periodic stress oscillations before the onset of weakening are caused by a sample misalignment of 5–10 μm . This is equivalent to changes of one or two grain sizes in the gouge layer generated in the shear zone during the course of the test. During the onset of strong dynamic weakening, LVDT data reveal that the shear zone is dilating by about 10 μm (Supplementary Fig. 9), consistent with the observed transient increases in normal stress (Supplementary Figs 8 and 9).

Numerical simulations were performed using the finite-element program Abaqus/Simulia²⁴.